

A short-pulse X-ray beamline for spectroscopy and scattering

R. Reininger,^{a*} E. M. Dufresne,^a M. Borland,^a M. A. Beno,^a L. Young^a and P. G. Evans^b

^aAdvanced Photon Source, Argonne National Laboratory, Argonne, IL 60439, USA, and ^bDepartment of Materials Science and Engineering, University of Wisconsin, Madison, WI 53706, USA. *E-mail: reininger@aps.anl.gov

Experimental facilities for picosecond X-ray spectroscopy and scattering based on RF deflection of stored electron beams face a series of optical design challenges. Beamlines designed around such a source enable time-resolved diffraction, spectroscopy and imaging studies in chemical, condensed matter and nanoscale materials science using few-picosecond-duration pulses possessing the stability, high repetition rate and spectral range of synchrotron light sources. The RF-deflected chirped electron beam produces a vertical fan of undulator radiation with a correlation between angle and time. The duration of the X-ray pulses delivered to experiments is selected by a vertical aperture. In addition to the radiation at the fundamental photon energy in the central cone, the undulator also emits the same photon energy in concentric rings around the central cone, which can potentially compromise the time resolution of experiments. A detailed analysis of this issue is presented for the proposed SPXSS beamline for the Advanced Photon Source. An optical design that minimizes the effects of off-axis radiation in lengthening the duration of pulses and provides variable X-ray pulse duration between 2.4 and 16 ps is presented.

Keywords: picosecond X-ray pulses; time-resolved spectroscopy and scattering; X-ray beamline.

© 2014 International Union of Crystallography

1. Introduction

Proposals for the generation of picosecond X-ray pulses using electron storage rings include the use of RF-deflection cavities to impose a correlation between the longitudinal position and the vertical momentum of each electron (Zholents *et al.*, 1999; Borland, 2005). In the particular design associated with the original upgrade of the Advanced Photon Source (APS), for example, one RF-deflection cavity located at the downstream end of a long straight section in Sector 5 generates chirped electron pulses and a second cavity at the downstream end of a long straight section in Sector 7 cancels the effect of the first cavity. The combined effect of the cavities was to create the desired time–angle correlation in sources located in Sectors 6 and 7 without affecting the electron beam at other locations in the storage ring. X-ray radiation emitted by insertion devices and bending magnets in these sectors would provide an ultra-stable, high-repetition-rate, widely tunable and polarized picosecond X-ray source, fully complementary to X-ray free-electron lasers (FELs). The large vertical divergence and the need to preserve the timing properties of the beam impose a series of optical design challenges that will be universal for sources making use of RF-deflection cavities to generate short pulses.

The X-ray radiation emitted when a chirped electron bunch traverses an undulator or bending magnet preserves the correlation imposed on the electron bunch by the RF cavities. A short X-ray pulse can be selected out using a pair of slits. We note that to date FELs operate in the regime of femtosecond pulse duration with

comparable time-averaged flux, but at considerably lower repetition rates and with less stability (Emma *et al.*, 2010; Ishikawa *et al.*, 2012). The experimental capabilities of the facilities based on the use of deflection cavities to generate picosecond X-ray pulses can address challenging problems in a wide range of fields, complementing probes available at FELs. The picosecond regime is the fundamental time-scale for a variety of phenomena for which new experimental insight will be crucial.

We describe here a beamline design based on an X-ray source enabled by RF-deflection cavities that allows variable pulse duration between 2.4 and 16 ps, continuous energy tunability between 4.7 and 35 keV, variable bandwidth with the choice of a double-crystal monochromator ($\Delta E/E \simeq 10^{-4}$) or multilayer monochromator ($\Delta E/E \simeq 10^{-2}$), variable X-ray repetition rate with the use of a mechanical chopper, and variable spot size down to a few micrometers when equipped with Kirkpatrick–Baez (KB) mirrors (Kirkpatrick & Baez, 1948).

The main goal of the particular RF-deflection cavity design in the original upgrade of the APS was to create a facility termed the Short-Pulse X-ray Source (SPX), comprising the cavities and associated X-ray experimental facilities. The SPX facility is not part of the initial scope of the current plan to upgrade the APS to a multi-bend achromat storage ring, and in fact cannot be implemented as originally designed. Nevertheless, we believe that some of the issues we addressed, and resolved, in the SPXSS beamline design are of general interest and particularly to those who may wish to implement a picosecond beamline based on Zholents' RF-orbit deflection

scheme (Zholents *et al.*, 1999). The beamline described here corresponds to the SPXSS beamline proposed to occupy the insertion device station of Sector 7 of the original APS upgrade. Similar optical issues are faced in the design of the proposed SPXIM [SPX imaging and microscopy (Reininger *et al.*, 2013a)] and the SPSXS [Short Pulse soft X-ray spectroscopy (Reininger *et al.*, 2013b)] beamlines.

2. Source

The simulations described below consider the propagation of the radiation emitted by an electron pulse, chirped by the RF cavity located in Sector 5, passing through a 27 mm-period 2.4 m-long undulator which is tuned to emit 10 keV. The center of the undulator is located 0.3 m upstream of the center of the APS 7-ID straight section.

The statistical representation of the radiation was obtained in four steps. In step (i) the accelerator simulation code *ELEGANT* (Borland, 2008) was used to determine the equilibrium properties of 10^6 electrons at the center of the undulator, sampling the horizontal and vertical phase space as well as time (position along the electron bunch). The electron energy spread ($<0.1\%$) was not included in the simulations since its contribution to the energy-dependent angular distribution is much smaller than the contribution due to the number of periods in the undulator. In step (ii) the angular distribution of the undulator radiation emitted at 10 keV from a single electron was obtained using the *SPECTRA* code (Tanaka & Kitamura, 2001) over a wide angular range. This range includes the first harmonic radiation at 10 keV, which is emitted in the forward direction ('central cone'), as well as the radiation nominally at 20 keV and emitted in a concentric ring to the central cone. The angular radius of the second harmonic (SH) ring, θ , was calculated (Kim, 1989) from $\theta = \gamma^{-1}(1 + k^2/2)^{1/2}$ where γ is the electron energy in units of mc^2 , m is the electron mass and c is the speed of light. Substituting the electron energy $\gamma (= 1.37 \times 10^4)$ and the undulator parameter $k (= 1.2)$ in the previous expression, one obtains $\theta = 96 \mu\text{rad}$. This means that the photon energy of the radiation emitted at $96 \mu\text{rad}$ is red-shifted from 20 keV down to 10 keV. Larger-radii ($>96 \mu\text{rad}$) concentric rings due to the red-shifted higher harmonics ($n > 2$) at 10 keV are also accepted by the beamline. In the calculations described here we did not include them because they are also filtered out as explained in §4 for the second harmonic. Since *SPECTRA* generates only the divergence of single electron emission, step (iii) involved a statistical sampling of the size of the central cone and that of the SH ring at the center of the insertion device. For the photon source size of the central cone radiation we assumed a Gaussian distribution with the standard RMS value (Elleume, 2003) of $\sigma = (2\lambda L)^{1/2}/2\pi = 3.9 \mu\text{m}$, where λ is the wavelength and L is the undulator length. The photon source size of the ring is considerably smaller as derived in the Appendix of Reininger *et al.* (2013a). That is, the size distribution of the SH radiation is approximately given by a Gaussian with a RMS value of $\sigma/(2N^{1/2}) = 0.2 \mu\text{m}$ where N is the number of undulator periods. We note that the product of the size of the SH ring and its angular radius is approximately $\lambda/(2\pi)$, as it is for the central cone radiation. In step (iv) the electron distribution [obtained in step (i)] was convoluted with the statistical sampling of the undulator radiation calculated in steps (ii) and (iii). The Advanced Photon Source standard 24-bunch mode with a 41 ps RMS electron bunch length were assumed in the *ELEGANT* calculation.

Fig. 1 shows the correlation between time and the vertical angle of the radiation emitted at 10 keV over the full horizontal fan of almost 400 μrad . We have chosen a logarithmic representation of the 10^6 rays

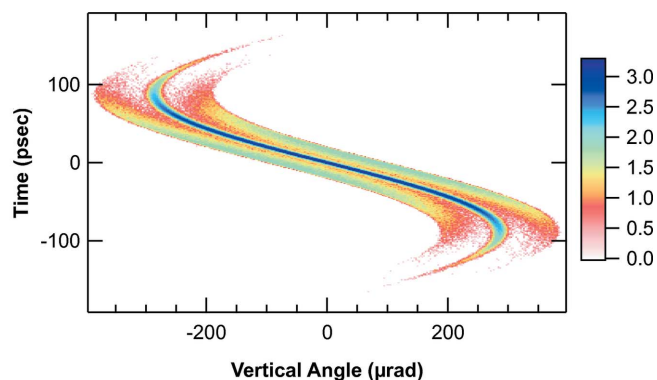


Figure 1

Log (base 10) of the number of rays as a function of time and vertical angle when accepting the full horizontal fan (see text).

in the figure to illustrate the correlation and to show the significant variation in the number of rays reaching different regions of the time-angle phase space. Fig. 2 shows the same correlation when the horizontal acceptance is limited to 50 μrad and therefore contains 23% fewer rays than Fig. 1. As seen in Fig. 2, and less clearly in Fig. 1, there are three bands. The central band corresponds to the radiation emitted by the undulator in the first harmonic whereas the other two bands correspond to the off-axis radiation due to the SH at an angle equal to $\pm 96 \mu\text{rad}$ as explained above. Evidently, the rays not accepted by the horizontal aperture are mostly those in the SH ring. The ratio of rays in the SH ring to those in the central cone are reduced from $\sim 29\%$ with full horizontal acceptance down to $\approx 3.5\%$ when the horizontal aperture is 50 μrad .

Fig. 2 demonstrates that the correlation between time (t) and vertical angle is almost linear for the first and SH radiation over approximately $\pm 200 \mu\text{rad}$ and $|t| < 45 \text{ ps}$ with a slope of $-0.2 \text{ ps } \mu\text{rad}^{-1}$. The time resolution in the limit of zero divergence for the radiation emitted in the central cone is determined by the properties of the electron beam and the divergence of the photon beam. Its value, 2.4 ps FWHM, is obtained from a narrow angular range around 0 μrad in the trace representing the central cone radiation in Fig. 2. However, it should be pointed out that the presence of the SH may produce an artifact since these photons arrive at $\pm 96 \mu\text{rad} \times 0.2 \text{ ps } \mu\text{rad}^{-1} = \pm 19 \text{ ps}$ for the same vertical angle. Another factor deteriorating the time resolution is the fraction of rays with $|t| > 40 \text{ ps}$ in the $\pm 200 \mu\text{rad}$ vertical angle range, due to electrons in the 'back-chirped' pulse. This effect is relatively small since the flux in the 'back-chirped' pulse is less than 0.04% of the total flux in the $\pm 130 \mu\text{rad}$ range.

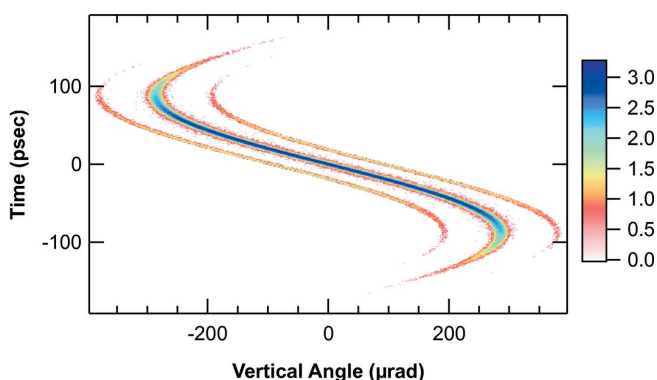


Figure 2

Log (base 10) of the number of rays as a function of time and vertical angle when accepting 50 μrad horizontally.

Table 1
Position of the optical elements relative to the straight section center.

Element	Position (mm)	Note
Undulator center	-300	
Horizontal source	0	
Vertical source	2590	
White-beam slits	26500	Up to 2 mm (H) × 2 mm (V)
Cylindrical mirror	27500	Vertical collimating
DCM	29500	
DMM	31500	
Cylindrical mirror	34000	Vertical focusing
Chopper/vertical slit	50000	
Elliptical cylinder	53500	Vertical focusing
Elliptical cylinder	54000	Horizontal focusing
Sample at C endstation	55000	
Elliptical cylinder	57750	Vertical focusing
Elliptical cylinder	58250	Horizontal focusing
Sample at D Endstation	58750	

An important point for any beamline design is to determine the longitudinal position of the source waist along the horizontal and vertical directions. For this particular source, we used the linear relationship between time and vertical angle to separate the rays of the first and SH radiation over the $\pm 130 \mu\text{rad}$ vertical angle range. The electron beam as well as the rays belonging to each band were then propagated (using ray-tracing) as a function of the longitudinal position relative to the center of the insertion device. Fig. 3 shows the standard deviation (SD) of the vertical sizes of the electron beam and of the three bands of the photon beam as a function of the longitudinal position. As seen in the figure, the vertical waist of the electron beam is located at ≈ 2.6 m from the center of the straight section as a consequence of the electron optics that include the RF cavity. The traces of the photon beams follow those of the electron beam and have their waists at approximately the same longitudinal position.

Each one of the traces in the figure was fitted with $\{[(x - x_0)\sigma']^2 + \sigma_0^2\}^{1/2}$, where x is the longitudinal position, σ' is the divergence, σ_0 and x_0 are the waist and its position. The fits yield $16 \mu\text{m}$, $22 \mu\text{m}$ and $19 \mu\text{m}$ for the waist of the electron beam, the central cone and the two bands due to the SH radiation, respectively. The waist position of the central cone and that of the electron coincide at 2.59 m (2.89 m) downstream of the center of the straight section (undulator) whereas the waist position of the early SH radiation is a few millimeters downstream and that of the late SH radiation is a few millimeters upstream. We note that an estimate for the waist of the central cone

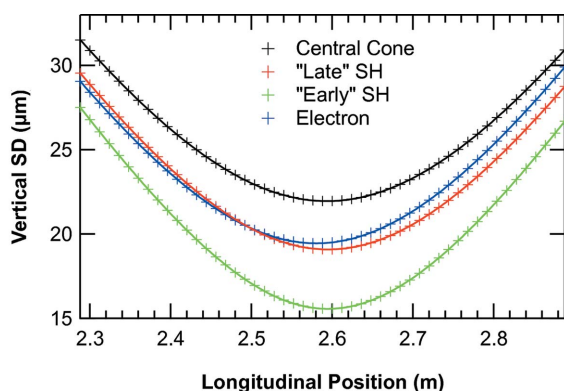


Figure 3
SD of the vertical size of the electron distribution (green) and its convolution with the photon beam (black: central cone; red: SH late pulse; blue: SH early pulse) as a function of the longitudinal distance. Zero meters corresponds to the center of the straight section. The undulator center is at -0.3 m from the center of the straight section.

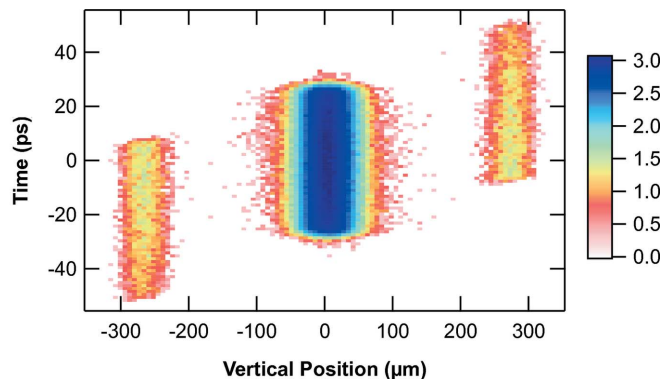


Figure 4
Log (base 10) of the number of rays as a function of time and vertical position at 2.59 m downstream from the center of the straight section, *i.e.* where the radiation has its vertical waist. The bands at $\approx 277 \mu\text{m}$ are due to the SH.

at 2.89 m from the undulator center, calculated from the square root of the sum of the squares (SRSS) of the electron waist with the RMS size of the single electron emission at $D = 2.89$ m, $\approx D[\lambda/(2L)]^{1/2}$, where L is the length of the insertion device, also yields $22 \mu\text{m}$. Very good agreement is also obtained between the value of the SH radiation waist given above and calculated using the SRSS of the electron waist and $D \times$ the height of the arc from the $96 \mu\text{rad}$ radius limited by $50 \mu\text{rad}$. The calculation for the horizontal SD of the photon beams yields a waist equal to $308 \mu\text{m}$, located at the center of the 7-ID straight section, the same values as that of the electron beam.

Fig. 4 shows the number of rays as a function of time and vertical coordinate at the position of the electron beam and central cone waists, *i.e.* at 2.89 m downstream from the center of the undulator. As in Figs. 1 and 2, we have chosen a logarithmic representation for the number of rays to show the three bands and the significant difference in the number of rays in the central cone and SH. Fig. 4 demonstrates that the center of the SH contributions are separated vertically from the center of the first harmonic radiation by $\pm 96 \mu\text{rad} \times (2.89) \text{ m} = \pm 277 \mu\text{m}$ with very little overlap. This important result means that a slit located at an image plane of the vertical waist significantly reduces the radiation of the SH which arrives at ± 19 ps for the same vertical angle.

3. Optical layout

Fig. 5 shows the optical layout of the SPXSS beamline. Table 1 summarizes the position of the optical elements relative to the center of the straight section.

A set of white-beam slits with a maximum aperture of $2 \text{ mm} \times 2 \text{ mm}$ (H \times V) is placed at 26.5 m from the center of the straight section. The pulse duration of the beamline is determined by the convolution between its vertical acceptance and the pulse duration of the source.

The first optical element of the beamline is a vertically deflecting meridional cylinder which collimates the photon beam along the vertical direction. This mirror is located at 27.5 m from the center of the straight section and it is water-cooled. The 1.2 m Si substrate was designed to have three reflecting coatings along its width, Pt, Rh and Si (SiO_2/Si), and to operate at an angle of 2 mrad . The collimated beam is then monochromated either by a vertically diffracting double-crystal monochromator (DCM) using Si (220) crystals or a double-multilayer crystal monochromator (DMM).

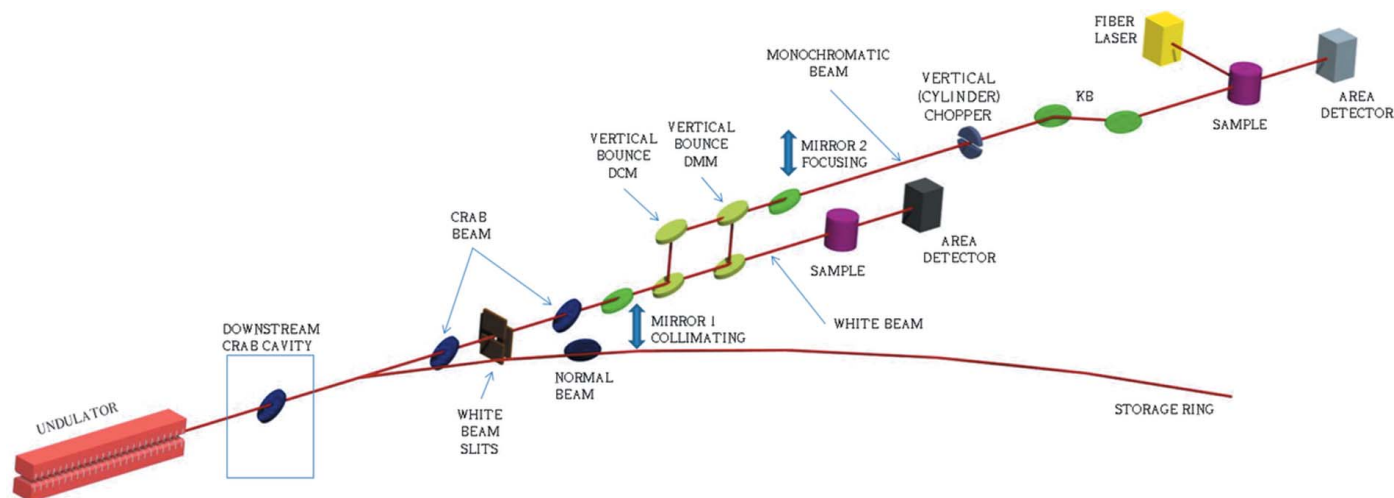


Figure 5
Optical layout of the SPXSS beamline.

The meridional cylinder downstream from the monochromator focuses the vertically collimated beam onto a slit located 16 m downstream from the mirror and very close to the chopper position. The mirror length, optical coatings and angle of incidence are the same as those of the collimating mirror. The vertical demagnification of the source along the vertical direction onto the slit by the two mirrors is close to 1.6.

The focusing onto the sample position at the two experimental stations, C and D, is performed with KB pairs. These 0.5 m-long bendable mirrors are designed to operate at angles of incidence between 2 and 6 mrad for high harmonics suppression. The first element of the KBs images the vertical slit at the sample position whereas the second element of each KB pair images the source along the horizontal direction. The geometrical demagnification of the vertically focusing elements in the KBs are 2.3 and 7.7 for the C and D stations, respectively. The corresponding values for the horizontal mirrors are 54 for the C station and 116 for the D station.

4. Ray-tracings

The ray-tracings described below were performed using the *SHADOW* code (Cerrina, 1984; Sanchez-del Rio *et al.*, 2011) in order to understand the effect of the slope errors on the optical components and the trade-offs due to the front aperture with respect to the pulse duration. The source used in the ray-tracings consisted of the 10^6 rays described in §2 having a continuous distribution of photon energies between 9.999 and 10.001 keV. In the first set of ray traces an aperture 26.5 m downstream from the center of the straight section was set to accept $1.2 \text{ mm} \times 2 \text{ mm}$ (H \times V). In the second set, the aperture was set to accept only $1.2 \text{ mm} \times 0.3 \text{ mm}$ (H \times V). RMS meridional slope errors of $1 \mu\text{rad}$ on the collimating and focusing mirrors and $0.5 \mu\text{rad}$ on the KB mirrors were included in all the calculations described below.

As discussed above, the large vertical acceptance required to collect the central cone of undulator radiation generated by the chirped electron pulse also includes the SH radiation. This has two implications: time resolution degradation and an energy shift of the SH relative to the central cone. The former has been explained in §2. The energy shift is due to the different angle of incidence at the crystals between the central cone and the SH. Since at the waist

position the SH is shifted vertically by $\pm 277 \mu\text{m}$ from the central cone radiation, its vertical angle after the collimating mirror and the DCM results in an energy shift of $\approx \pm 0.35 \text{ eV}$.

The vertical separation between the central cone and SH radiation is actually the solution for filtering the SH: a slit at the vertical image, *i.e.* at the focus of the second mirror, should be able to block practically all the SH radiation. The use of a slit to block the SH radiation is demonstrated in Fig. 6, which shows the correlation between time and vertical divergence for two cases: with and without a $120 \mu\text{m}$ vertical slit. We note that, since the rings due to the higher harmonics (also red-shifted to 10 keV) have larger radii than the SH, they are also filtered by the vertical slit.

The histograms representing the pulse duration with and without the slit derived from the data in Fig. 6 are shown in Fig. 7. The FWHM of the pulse, 16 ps (see Fig. 7), is not reduced by the slit. This figure also shows that the slit blocks the contributions of the SH radiation that is seen in the time intervals between ± 12 and ± 20 ps. The first-harmonic radiation lost due to the slit can be obtained from the ratio of the integrated area below the traces in Fig. 7 between -10 and 10 ps. The loss in the first-harmonic intensity is $\approx 25\%$ and it is mainly due to the broadening of the beam at the slit plane resulting from the slope errors on the first two mirrors. Evidently, smaller slope errors on the mirrors would reduce the flux losses.

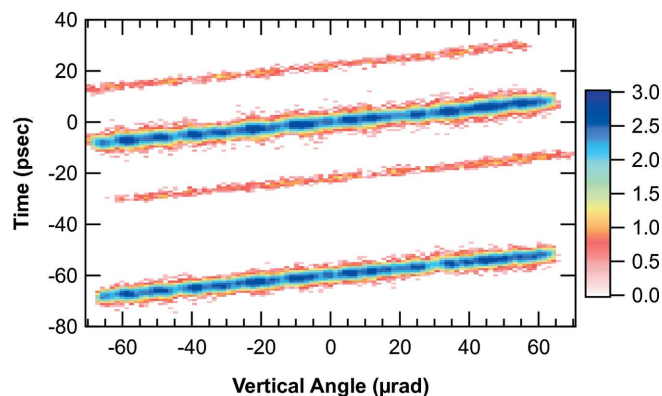


Figure 6
Log (base 10) of the number of rays at the slit position as a function of time and vertical angle. Upper three bands (centered around 0 ps): without a slit; lower band (shifted by -60 ps to make it visible in the figure): with a $120 \mu\text{m}$ slit.

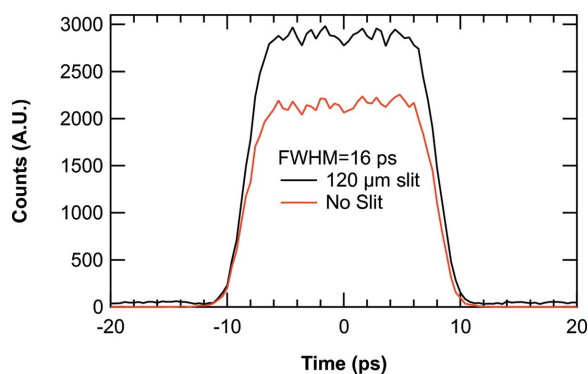


Figure 7 Pulse duration without (black trace) and with (red trace) a 120 μm slit. 1 μrad RMS slope error on the first two mirrors, 2 mm vertical acceptance.

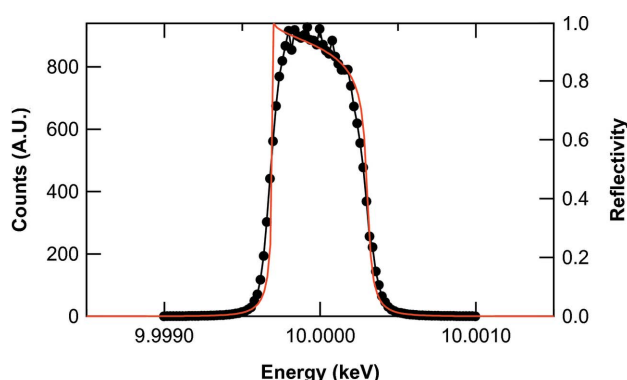


Figure 8 Energy resolution obtained from the ray-tracings (black circles). Right axis and red trace: reflectivity of two flat Si220 crystals with collimated light.

Fig. 8 compares the resolution of a perfectly collimated beam incident on the monochromator with the one obtained from the ray-tracings after the exit slit. As the figure demonstrates, the figure errors on the collimating mirror have a minimal effect on the energy resolution; there is some broadening at the base of the trace derived from the ray tracings but the FWHM stays the same as in the ideal case, 0.61 eV.

The above results were obtained with a 2 mm vertical aperture. Shorter pulse duration can be obtained at the expense of flux by reducing the vertical acceptance of the beamline. With a 0.3 mm vertical aperture (11 μrad) the pulse duration should be given approximately by $[(11 \mu\text{rad} \times 0.2 \text{ ps } \mu\text{rad}^{-1})^2 + (2.4 \text{ ps})^2]^{1/2} = 3.3 \text{ ps}$. This is actually the FWHM of the pulse duration obtained with the 0.3 mm aperture from figures equivalent to Figs. 6 and 7.

The flux density calculated at the sample position of station D at 10 keV, for a 2 mm vertical aperture, a 120 μm slit, an energy resolution of 0.61 eV and including the slope errors quoted at the beginning of this section is shown in Fig. 9. The RMS values obtained from the ray-tracings and quoted in the figure are 2.7 μm × 4.2 μm (H × V). The RMS size along the horizontal direction including the geometrical demagnification and the meridional slope errors of the second mirror of the KB pair is 2.6 μm, in agreement with the result in Fig. 9. The histogram in the figure for the vertical direction shows that a Gaussian is not a good representation of the profile since along this direction the mirror is focusing the beam that passes through a 120 μm slit. For a pure slit one would expect a square profile of $120/7.7 = 15.6 \mu\text{m}$, consistent with the histogram in the figure when one takes into account the slope errors on the mirror. Table 2

Table 2

Flux, sizes, divergences and time resolution at the sample position at 10 keV with 0.61 eV resolution.

Values of size, divergence and time resolution are FWHM.

Station	Aperture (mm)	Flux (photons s ⁻¹)	Sizes (μm)	Divergences (mrad)	Time (ps)
C station	2.0	1.0×10^{12}	13 × 42	1.7 × 0.23	16
D station	2.0	1.0×10^{12}	5.8 × 13	3.5 × 1	16
C station	0.3	1.7×10^{11}	13 × 24	1.7 × 0.09	3.3
D station	0.3	1.7×10^{11}	5.8 × 9.4	3.5 × 0.18	3.3

summarizes the calculated flux, RMS sizes and divergences as well as pulse duration in stations C and D at an energy of 10 keV and a resolution of 0.61 eV.

5. Discussion

One of the requirements to eliminate the SH contamination in the photon pulse is that the position of the electron vertical waist must not coincide with the center of the undulator. Since at high photon energies the size of the single electron emission is smaller than the size of the electron beam along the vertical direction, the position of the photon beam vertical waist (convoluted with the electron beam) is very close to that of the electron vertical waist. At this position the SH radiation is in a ring with a radius $D\theta$, where D is the distance between the undulator center and the position of the beams waist. If the first and second harmonics are well separated at this position, the horizontal acceptance is reduced to accept the width of the first-harmonic photon beam, and the figure errors of the cylindrical mirrors are less than a certain value, then a vertical slit in the beamline will effectively remove the SH radiation. As shown above, these conditions were fulfilled in the original design and could be fulfilled at other synchrotron radiation facilities interested in a beamline capable of generating picosecond pulses.

SPXSS and two other beamlines designed to deliver picosecond pulses, SPXIM (Reininger *et al.*, 2013a) and SPSXS (Reininger *et al.*, 2013b), were conceived for the original APS upgrade that included the SPX source and facility. This RF-based source required a 7.7 m-long straight section, and 2.7 m-long cryostats to produce the 2 MV for the deflection of the electron beam (Nassiri *et al.*, 2012; Xiao *et al.*, 2012). The APS is currently planning an upgrade based on a multi-

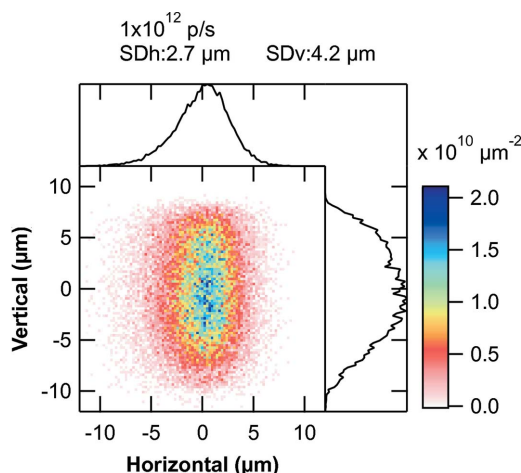


Figure 9 Flux density (scale in units of photons s⁻¹ μm⁻²) at the sample position at the energy resolution of the Si(220) DCM for a 2 mm vertical aperture (16 ps pulse length).

bend achromat (MBA) lattice that would reduce significantly the electron beam emittance by approximately two orders of magnitude. Long straight sections are not planned in the MBA lattice, thus the original crab-cavity-based technology (Nassiri *et al.*, 2012) cannot be implemented.

However, shorter cavities based on a quasi waveguide multi-cell resonator (QMIR) are being explored (Zholents & Ostrumov, 2013). This compact superconducting technology could produce a picosecond source self-contained in a single straight section. A design using four 0.5 m QMIR cavities and two 1.2 m 19 mm-period superconducting undulators has been explored. In this design, each half of the straight section contains one undulator enclosed by two cavities. Calculations were performed with this conceptual picosecond electron source assuming horizontal and vertical emittances equal to 60 pm and 6 pm, respectively. Using these parameters we simulated the photon beam as described in §2. The vertical waists of the electron beam, the first harmonic and the second harmonic were found at the same distance from the undulator (0.95 m). This ensures that the second harmonic contamination can be filtered at the slit with RMS slope errors on the two cylindrical mirrors $\lesssim 0.5 \mu\text{rad}$. The horizontal source size in the simulated lattice is more than ten times smaller than the present APS. Therefore, a micrometer-size spot size could be easily achieved in station D by changing the order of the vertical and horizontal mirrors in the KB pair. A detailed design of the QMIR source and its associated beamline will be required after the MBA lattice has been commissioned. Furthermore, detailed simulations will have to show the negligible effect of the picosecond source on the performance of the MBA lattice ensuring that the system is transparent to the other APS users. The new facility could provide exquisite pump-and-probe experiments at a stable high-repetition-rate synchrotron source with nearly round focused X-ray beams on few-picoseconds time scales.

6. Conclusion

The SPXSS beamline was designed to provide a pulse duration between 2.4 and 16 ps, continuous energy tunability between 4.7 and 35 keV, variable bandwidth with the choice of a double-crystal monochromator ($\Delta E/E \simeq 10^{-4}$) or multilayer monochromator ($\Delta E/E \simeq 10^{-2}$), variable X-ray repetition rate with the use of a mechanical chopper, and variable spot size down to a few micrometers when equipped with KB mirrors. The beamline as described

in this paper will not be part of the APS upgrade. However, the beamline requirements for extracting clean picosecond-duration pulses from a chirped electron beam for implementation at other synchrotron sources, or at the APS in a later upgrade, are discussed in detail.

The Advanced Photon Source, an Office of Science User Facility operated for the US Department of Energy (DOE) Office of Science by Argonne National Laboratory, was supported by the US DOE under Contract No. DE-AC02-06CH11357. LY acknowledges support from the US Department of Energy (DOE) Office of Science, Division of Chemical, Geological and Biological Sciences under Contract No. DEAC02-06CH11357. PE acknowledges support from the US Department of Energy, Office of Basic Energy Sciences, Division of Materials Sciences and Engineering under Grant No. DE-FG02-10ER46147. We thank Mark Erdmann and Joshua Downey for their contribution to the beamline layout.

References

- Borland, M. (2005). *Phys Rev ST Accel. Beams*, **8**, 074001.
- Borland, M. (2008). *Elegant: A Flexible SDDS-Compliant Code for Accelerator Simulation*, http://www.aps.anl.gov/Science/Publications/lnotes/content/files/APS_1418218.pdf.
- Cerrina, F. (1984). *Proc. SPIE*, **503**, 68–77.
- Elleaume, P. (2003). In *Undulators, Wigglers and their Applications*, edited by H. Onuki and P. Elleaume. London: Taylor and Francis.
- Emma, P. *et al.* (2010). *Nat. Photon.* **4**, 641–647.
- Ishikawa, T. *et al.* (2012). *Nat. Photon.* **6**, 540–544.
- Kim, K.-J. (1989). *AIP Conf. Proc.* **184**, 565–632.
- Kirkpatrick, P. & Baez, A. V. (1948). *J. Opt. Soc. Am.* **38**, 766–774.
- Nassiri, A. *et al.* (2012). *Proceedings of IPAC'12*, New Orleans, LA, USA, pp. 2292–2294.
- Reininger, R., Dufresne, E. M., Borland, M., Beno, M. A., Young, L., Kim, K.-J. & Evans, P. G. (2013a). *Rev. Sci. Instrum.* **84**, 053103.
- Reininger, R., Keavney, D. J., Borland, M. & Young, L. (2013b). *J. Synchrotron Rad.* **20**, 654–659.
- Sanchez del Rio, M., Canestrari, N., Jiang, F. & Cerrina, F. (2011). *J. Synchrotron Rad.* **18**, 708–716.
- Tanaka, T. & Kitamura, H. (2001). *J. Synchrotron Rad.* **8**, 1221–1228.
- Xiao, L., Li, Z., Ng, C., Nassiri, A., Waldschmidt, G., Wu, G., Wang, H. & Rimmer, R. (2012). *Proceedings of IPAC2012*, New Orleans, LA, USA, pp. 2414–2416.
- Zholents, A., Heimann, P., Zolotarev, M. & Byrd, J. (1999). *Nucl. Instrum. Methods Phys. Res. A*, **425**, 385–389.
- Zholents, A. A. & Ostrumov, P. (2013). Personal communication.